J|A|C|S ARTICLES

Published on Web 04/06/2009

Spectroscopic and Kinetic Evidence on How Bacteriorhodopsin Accomplishes Vectorial Proton Transport under Functional Conditions

Víctor A. Lórenz-Fonfría*,‡ and Hideki Kandori

Department of Frontier Materials, Nagoya Institute of Technology, Showa-ku, Nagoya 466-8555, Japan

Received January 16, 2009; E-mail: victor.lorenz@gmail.com

Abstract: Vectorial transport by pumps requires a switch in the accessibility (or affinity) of the ion binding site from the extracelullar to the cytoplamic side, or *vice versa*. In the proton-pump bacteriorhodopsin (bR) the nature of this *switch* mechanism is still controversial, although it is expected to occur during the transition between two M substates. Here, we characterized this transition by time-resolved Fourier transform infrared (FT-IR) spectroscopy under functional conditions, using a novel approach for the analysis of kinetic data: *the regularized inversion of an eigenvalue problem*. The use of IR spectroscopy allowed the simultaneous evaluation of the involvement of the protein backbone, retinal, amino acid side chains, and internal water molecules in the *switch* mechanism. We provide solid evidence that the *switch* is not associated with protein backbone conformational changes. On the other hand, changes in the retinal conformation (or in the orientation of the Schiff Base (SB) during the *switch*) are reasonably although not completely discarded. We found that the proton release group (PRG), a delocalized proton characterized by a broad continuum band in the infrared, deprotonates in the transition between two M substates. Vectorial proton transport is most likely guaranteed by the coupled proton affinity changes resulting from the PRG deprotonation, favoring an affinity-based over an accessibility-based *switch* mechanism.

1. Introduction

Transport of ions and molecules against their electrochemical membrane potential gradient is mediated by membrane active transporters. In the primary active transporters this thermodynamically unfavorable process is coupled to light absorption, electron transfer, or ATP-hydrolysis, while in the secondary transporters it is coupled to the movement of a second solute down its membrane potential gradient.[1,2] In spite their fundamental differences, both types of transporters require a mechanism switching or gating the ion/substrate binding site from the extracellular (EC) to the cytoplasmic (CP) side, or *vice versa*, in order to avoid a short circuit and to allow an effective coupling of the input energy into vectorial active transport.[1,3,4]

The actual difficulties and ambiguities that can be encountered when trying to reveal the *switch* mechanism of an active transporter are perfectly manifested in bacteriorhodopsin (bR), intensely characterized from both the functional and structural point of view.[5,6] In the proton-pump cycle of bR (Figure 1), the CP-to-EC proton transport vectoriality is mostly a consequence of the deprotonation/protonation sequence of the retinal

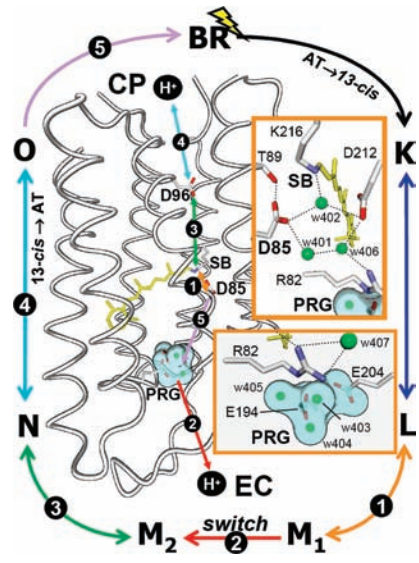

Figure 1. Schematic representation of the bacteriorhodopsin (bR) photocycle, showing the main processes between intermediates: light-induced retinal isomerization from *all-trans* to 13-*cis* and its recovery; the *switch* step (between two M substates); and five proton transfers. The five proton transfers are represented overlaid on a structural model of the bR ground state (pdb 1c3w[84]). The inserts show a rotated and more detailed view of the SB region (top) and proton release group (PRG) region (bottom). Some important internal water molecules are displayed as green spheres. Some potential H-bonds are indicated with dashed lines.

Schiff Base (SB), the "substrate-binding site". In the L-to-M transition, a proton is transferred from the SB to Asp85, the

‡ Present address: Unitat de Biofísica, Departament de Bioquímica i de Biologia Molecular, Universitat Autònoma de Barcelona, Barcelona 08193, Spain.

(1) Lanyi, J. K.; Pohorille, A. *Trends Biotechnol.* **2001**, *19*, 140–144.
(2) DeFelice, L. J. *Trends Neurosci.* **2004**, *27*, 352–359.
(3) Brzezinski, P. *Trends Biochem. Sci.* **2004**, *29*, 380–387.
(4) Locher, K. P.; Bass, R. B.; Rees, D. C. *Science* **2003**, *301*, 603–604.
(5) Haupts, U.; Tittor, J.; Oesterhelt, D. *Annu. Rev. Biophys. Biomol. Struct.* **1999**, *28*, 367–399.
(6) Lanyi, J. K. *Annu. Rev. Physiol.* **2004**, *66*, 665–688.

EC proton acceptor. In the M-to-N transition, the SB recovers the proton from Asp96, the CP proton donor. Some directional processes should occur while the SB is deprotonated, preventing the SB reprotonation back from Asp85, and forcing the SB to remain unprotonated until Asp96 becomes available as a CP proton donor. There is unanimous agreement that this requires at least two substates with a deprotonated SB: a pre and post-*switch* M substate.[5,6]

There is, however, a fundamental disagreement about what constitutes the *switch* mechanism in the proton-pump cycle of bR. Likely hypotheses are: (i) a protein conformational change (tilt of some helices), closing/opening the access of the SB to the EC/CP domains,[7,8] or inhibiting the proton back-flow from Asp85 to the SB by increasing their distance;[9] (ii) relaxation of the retinal torsion, leading to the EC-to-CP reorientation of the SB, away from Asp85;[6,10] (iii) a change in the curvature of the retinal, moving the SB away from Asp85, slowing down the proton back-flow;[11] (iv) a change in the number and/or the location of the internal waters involved in the proton transfer from the SB to the Asp85, inhibiting kinetically the proton back-flow;[12,13] (v) deprotonation of the proton release group (PRG) coupled with an increase of Asp85 pK_a (proton affinity), making the reprotonation of the SB from it energetically unfavorable.[14]

Most of what it is known about the *switch* mechanism in bR has been deduced by artificially enhancing the accumulation of M substates. This has been accomplished using extreme sample conditions (low temperature, high pH, molar concentrations of various chemicals, etc.) and/or mutants with altered photocycles,[5,15] with the risk of "trapping" artificial intermediates and loosing functional relevance. Instead, a rigorous examination of the functional *switch* mechanism requires the temporal resolution of the transition between the M substates in the wild-type bR photocycle, ideally by the use of a time-resolved method sensitive to all of the above-described potential players in the *switch*.

Such a study is presented here, using time-resolved infrared difference spectroscopy with microsecond time resolution. Unlike previous time-resolved UV−vis or Raman spectroscopy studies, mostly sensitive to changes in the retinal and the protonation state of the SB,[16,17] IR spectroscopy provides simultaneous insight on changes in the protein backbone, retinal, SB, amino acid side chains, and internal water molecules.[18] To solve the known ambiguities inherent to the resolution of intermediates from time-resolved data,[19,20] we introduce a conceptually simple, yet powerful, analytical method: *the regularized inversion of an eigenvalue problem*, inspired in lessons learned in the field of inverse theory.[21]

The successful resolution of the transition between two M substates reveals that the *switch* mechanism in bR does not rest on protein backbone conformational changes, and most likely not in changes in the retinal conformation or in the SB reorientation either. Instead, the *switch* mechanism is likely provided by the unidirectional deprotonation of the PRG in the transition between two M substates, coupled to an increase of the proton affinity of Asp85.

2. Methods

Time-Resolved Step-Scan FTIR Spectroscopy. Approximately 60 μL of bR in the purple membranes (2 mM KP_i at pH 7.0) were dried over a BaF_2 window of 2.5 mm diameter, and hydrated to a relative humidity of ~92%.[22] This reduced humidity prevents saturation of the O−H stretching region by the bulk water,[22] slightly slowing down the transition between M subtates and favoring its characterization, but without presumably altering the normal photocycle.[23] Time-resolved step-scan FTIR experiments of the bR photocycle were performed at 20.0 °C, recorded at 8 cm^{-1} resolution from 2.5 μs to 13 ms, as described in detail elsewhere.[22]

Singular Value Decomposition (SVD). A detailed description of SVD basis and applications can be found elsewhere.[24−26] SVD was performed on the experimental time-resolved data matrix, $\mathbf{D}$ ($n_v \times n_t$), using the "svd" Matlab function, but with some modifications to respect typical implementations. SVD decomposes the data into orthonormal abstract spectra and time-traces: $\mathbf{D} = \mathbf{V} \times \mathbf{S} \times \mathbf{U}$, where $\mathbf{V}$ ($n_v \times n_t$) is the abstract spectra matrix, $\mathbf{U}$ ($n_t \times n_t$) is the abstract time-trace matrix, and $\mathbf{S}$ ($n_t \times n_t$) is a diagonal matrix containing in its diagonal, $\mathbf{s}$ ($n_t \times 1$), the singular values. For noiseless data, the number of spectroscopic and kinetic independent intermediates can be obtained from n_s, the number of not null elements in $\mathbf{s}$. For data with normally random noise, the singular values will not be zero above the expected value of n_s but decay approximately exponentially. If the n_s singular value for the data in the absence of noise is significantly higher than the n_s singular value of the noise, then the last signal component, n_s, will be determined correctly, as so the number of mathematically independent intermediates. Besides random noise, experimental time-resolved data often contain baseline fluctuations. Unlike random noise, the singular value associated to the baseline fluctuations can be quite high, leading to an overestimation of n_s. Even more important, the baseline fluctuations will become mixed with the abstract spectra and the time-traces, thus lowering their quality. A way we devised to decrease to the minimum this pernicious effect was to preprocess the experimental data, performing the first derivative as a function of the wavenumber. The first derivative completely cancels offset fluctuations and effectively minimizes more complex baselines fluctuations. We also took proper account of the expected noise dependence on wavenumber and time. Therefore, SVD was performed on $\mathbf{D_w}' = diag(\mathbf{w_t}) \times der[\mathbf{D}] \times diag(\mathbf{w_v})$, where $\mathbf{w_v}$ ($n_v \times 1$) and $\mathbf{w_t}$ ($n_t \times 1$) elements

(7) Sass, H. J.; Schachowa, I. W.; Rapp, G.; Koch, M. H.; Oesterhelt, D.; Dencher, N. A.; Büldt, G. *EMBO J.* **1997**, *16*, 1484–1491.
(8) Subramaniam, S.; Lindahl, M.; Bullough, P.; Faruqi, A. R.; Tittor, J.; Oesterhelt, D.; Brown, L.; Lanyi, J.; Henderson, R. *J. Mol. Biol.* **1999**, *287*, 145–161.
(9) Neutze, R.; Pebay-Peyroula, E.; Edman, K.; Royant, A.; Navarro, J.; Landau, E. M. *Biochim. Biophys. Acta* **2002**, *1565*, 144–167.
(10) Herzfeld, J.; Lansing, J. C. *Annu. Rev. Biophys. Biomol. Struct.* **2002**, *31*, 73–95.
(11) Subramaniam, S.; Henderson, R. *Nature (London)* **2000**, *406*, 653–657.
(12) Bondar, A. N.; Suhai, S.; Fischer, S.; Smith, J. C.; Elstner, M. *J. Struct. Biol.* **2007**, *157*, 454–469.
(13) Tanimoto, T.; Furutani, Y.; Kandori, H. *Biochemistry* **2003**, *42*, 2300–2306.
(14) Richter, H. T.; Brown, L. S.; Needleman, R.; Lanyi, J. K. *Biochemistry* **1996**, *35*, 4054–4062.
(15) Betancourt, F. M.; Glaeser, R. M. *Biochim. Biophys. Acta* **2000**, *1460*, 106–118.
(16) Lanyi, J. K.; Váró, G. *Isr. J. Chem.* **1995**, *35*, 365–385.
(17) Mathies, R. A.; Lin, S. W.; Ames, J. B.; Pollard, W. T. *Annu. Rev. Biophys. Biophys. Chem.* **1991**, *20*, 491–518.
(18) Maeda, A. *Isr. J. Chem.* **1995**, *35*, 387–400.
(19) Nagle, J. F. *Biophys. J.* **1991**, *59*, 476–487.
(20) Dioumaev, A. K. *Biophys. Chem.* **1997**, *67*, 1–25.
(21) Hansen, P. C. *Rank-deficient and discrete ill-posed problems: Numerical aspects of linear inversion*; SIAM: Philadelphia, 1998.
(22) Lórenz-Fonfría, V. A.; Furutani, Y.; Kandori, H. *Biochemistry* **2008**, *47*, 4071–4081.
(23) Váró, G.; Lanyi, J. K. *Biophys. J.* **1991**, *59*, 313–322.
(24) Press, W. H.; Teukolsky, S. A.; Vetterling, W. T.; Flannery, B. P. Numerical recipes in C. In *The art of scientific computing*, 2nd ed.; Cambridge University Press: New York, 1992.
(25) Hendler, R. W.; Shrager, R. I. *J. Biochem. Biophys. Methods* **1994**, *28*, 1–33.
(26) Henry, E. R.; Hofrichter, J. *Methods Enzymol.* **1992**, *210*, 129–192.

are the inverse of the expected noise standard deviation as a function of the wavenumber and time, *diag*() is a diagonal matrix with diagonal elements given by the vector in the brackets, and *der*[ ] performs the first derivative on the corresponding matrix columns. The first derivative was performed in the Fourier domain as described,[27,28] without apodization or phase correction. Then, the output of SVD becomes: $\mathbf{D_w}' = \mathbf{V_w}' \times \mathbf{S} \times \mathbf{U_w}$, and the normal **U** and **V** matrices can be recovered as $\mathbf{U} = \mathbf{U_w} \times (diag(\mathbf{w_t}))^{-1}$ and $\mathbf{V} = int[(diag(\mathbf{w_v}))^{-1} \times \mathbf{V_w}]$, where *int*[ ] performs the integral on the corresponding matrix columns. This process effectively pushes singular values associated to baseline fluctuations below those for genuine signals.

Global Exponential Fitting. It was performed on the first five abstract time-traces, in a homemade program[29] written in MATLAB version 7 (The Math Works, Natick, MA). In the global fitting we took into account the noise standard deviation dependence on time as well as the singular value associated to each abstract time-trace.[30]

Kinetic Analysis. The time-resolved data for the photocycle, **D** ($n_w \times n_t$), can be expressed in matrix notation as: $\mathbf{D} = \mathbf{S} \times \mathbf{C}^\mathbf{T}$, where **S** ($n_w \times n_i$) contains intermediates difference spectra, and **C** ($n_t \times n_i$) the intermediates fractions to respect time. **C** depends on the kinetic model and initial conditions, as: $\mathbf{C} = \exp(\mathbf{t} \times \boldsymbol{\alpha}^\mathbf{T}) \times \mathbf{X} \times \mathbf{F}$, where **t** ($n_t \times 1$) is the time; and **X** ($n_i \times n_i$) and $\boldsymbol{\alpha}$ ($n_i \times 1$) are the eigenvectors and eigenvalues, respectively, obtained after solving the eigenvalue problem $\mathbf{K} \times \mathbf{X} = \boldsymbol{\alpha} \times \mathbf{X}$.[20,29] The matrix **K** ($n_i \times n_i$) is the kinetic matrix constructed with the intrinsic rate constants of the kinetic scheme, and **F** ($n_i \times n_i$) is a diagonal matrix with diagonal elements given by $\mathbf{X}^{-1} \times \mathbf{c}_0$, where $\mathbf{c}_0$ ($n_i \times 1$) is a column vector containing the initial intermediates concentrations or fractions. Note: exp(**A**) represents here not the exponential of **A** but the exponential of **A** elements; and n_w, n_t, and n_i are the number of wavenumbers, time values, and intermediates, respectively. The experimental data will be given by: $\mathbf{D} = \mathbf{S} \times \mathbf{X} \times \mathbf{F} \times \exp(\boldsymbol{\alpha} \times \mathbf{t}^\mathbf{T})$, where **S**, and **X** and $\boldsymbol{\alpha}$ are unknown. From the macroscopic rate constant determined by global exponential fitting, $\mathbf{k^*}$ ($n_i \times 1$), we have an estimate of the eigenvalues of the kinetic matrix: $\boldsymbol{\alpha} \approx -\mathbf{k^*}$. An estimate of the eigenvectors **X** of the kinetic matrix from the decay-associated spectra determined by global exponential fitting, **B** ($n_w \times n_i$), is not directly obtainable, since $\mathbf{X} \approx \mathbf{S}^{-1} \times \mathbf{B} \times \mathbf{F}^{-1}$, but **S** is also unknown. Therefore, direct estimate of the **K** is not possible. Instead, **K** has to be indirectly estimated from the approximate knowledge of the eigenvalues and some extra information about the solution. This represents an inverse eigenvalue problem.[31] To estimate **K**, we first define a kinetic scheme. A possible solution should fulfill that $\boldsymbol{\alpha} \approx -\mathbf{k^*}$, but this condition alone is insufficient to provide a well-defined solution. To remove/attenuate any remaining ambiguity in the inversion problem, as well as to rule out unphysical and implausible solutions, we added a secondary convex goal, as is habitually done in inverse theory.[21] The intrinsic rate constants were also adjusted to approximately reproduce, to a scaling factor, the kinetics of some bands known to be fairly selective for the different intermediates in the photocycle,[22] $\mathbf{C}^{\exp}$ ($n_t \times n_i$), shown in the Supporting Information, Figure S1. This was done by adding the constraint: $\mathbf{C}_i \approx \mathbf{C}_i^{\exp} \times ((\mathbf{C}_i^\mathbf{T} \times \mathbf{C}_i)^{-1}\ \mathbf{C}_i^\mathbf{T} \times \mathbf{C}_i^{\exp})^{-1}$, where $\mathbf{C}_i$ is a $n_t \times 1$ vector from the column *i* of **C**, and $((\mathbf{C}_i^\mathbf{T} \times \mathbf{C}_i)^{-1}\ \mathbf{C}_i^\mathbf{T} \times \mathbf{C}_i^{\exp})^{-1}$ gives the least-squares proportionality factors between **C** and $\mathbf{C}^{\exp}$ columns. Therefore, the function minimized to obtain the not-null elements of **K** in logarithmic scale, included in a vector **a**, was:

$$Q(\mathbf{a}) = \|\log(\boldsymbol{\alpha}) + \log(\mathbf{k^*})\| + \lambda \times \sum_{i=1}^{n_i} \|diag(\mathbf{w_t}) \times \left[\mathbf{C}_i - \mathbf{C}_i^{\exp}\left((\mathbf{C}_i{}^T\mathbf{C}_i)^{-1}\mathbf{C}_i{}^T \times \mathbf{C}_i^{\exp}\right)\right]^{-1}\| \quad (1)$$

where λ is a regularization parameter, which balances both minimization goals. Based on probability considerations, the value of λ should be taken as the square of the ratio of the expected error of both terms: $\lambda = (\sigma_{\log k^*}/\ \sigma_{\mathrm{Cexp}})^2$. We took $\sigma_{\log k^*}$ as the average standard error of $\log(\mathbf{k^*})$, as provided by global exponential fitting, i.e., ~0.04. We assigned a value for σ_{Cexp} of 0.13. This means that as long as our scaled intermediate experimental kinetics do not differ from the real intermediate fractions by more than 0.13 (after weighing for $\mathbf{w_t}$), we should not expect to introduce any significant bias in the estimated intrinsic rate constant. Indeed, the solution obtained fulfilled such condition (see the residuals in the Supporting Information, Figure S1). The minimization of eq 1 was performed using a Newton−Gauss−Marquardt algorithm.[24] Briefly, a vector containing the intrinsic rate constants in logarithmic scale, $\mathbf{a}_{new}$, was iteratively updated from a previous vector, $\mathbf{a}_{old}$, as: $\mathbf{a}_{new} = \mathbf{a}_{old} + (\mathbf{J_Q}^\mathbf{T}\mathbf{J_Q} + \delta \times \mathbf{I})^{-1} \times \mathbf{J_Q}^\mathbf{T} \times \mathbf{r}$, where $\mathbf{J_Q}$ is the Jacobian matrix of Q residuals at $\mathbf{a}_{old}$, **I** is the identity matrix, δ is a scalar that assures that $Q(\mathbf{a}_{new}) \leq Q(\mathbf{a}_{old})$ and makes the minimization algorithm immune to possible singularities of $(\mathbf{J_Q}^\mathbf{T}\mathbf{J_Q})^{-1}$, and **r** is a vector containing the residuals of the two terms in eq 1 at $\mathbf{a}_{old}$. The derivatives of Q to respect **a** elements needed to construct the Jacobian matrix were computed numerically, perturbing **a** elements by 0.001 one by one and computing the resulting changes in the value of Q. Convergence was declared when Q changed by less than a 10^{-4} fraction in two consecutive iterations, and aborted if convergence was not obtained after 1000 iterations, or any intrinsic rate constant took values outside the expected interval (above $(100\ \mathrm{ns})^{-1}$ or below $(100\ \mathrm{ms})^{-1}$). We confirmed that the solution obtained did not vary when 10^3 successful (i.e., not aborted) minimizations starting from randomly generated initial guesses for the intrinsic rate constants were tested, strongly suggesting that Q has a unique well-defined minimum in the physical interval expected for the intrinsic rate constants (see Supporting Information, Figure S2). Asymptotic standard errors for **a** were calculated as: $\boldsymbol{\sigma}_\mathbf{a} = std(\mathbf{r})\ (diag(\mathbf{J_Q}^\mathbf{T}\mathbf{J_Q})^{-1})^{0.5}$, where **r** and $\mathbf{J_Q}$ were computed at the converged solution, *std*() computes the standard deviation, and *diag*() extracts the diagonal elements of a matrix.[32] The same procedure was used to estimate the errors of the equilibrium and relaxation rate constants (see Table 1). Note that these asymptotic errors assume that $Q(\mathbf{a})$ is well-approximated by a quadratic function at its minimum, which may not the case for some intrinsic rate constants. Once the elements of **a** were estimated, **K** was constructed. Then, **C** was computed as described above, and the pure intermediate difference spectra matrix was obtained as: $\mathbf{S}^\mathbf{T} = (\mathbf{C}^\mathbf{T}\mathbf{C})^{-1}\mathbf{C}^\mathbf{T} \times \mathbf{D}^\mathbf{T}$. Asymptotic errors for the estimated intermediate fractions, **C** columns, were calculated by linear propagation of the asymptotic errors of **a**, as $\boldsymbol{\sigma}_{\mathbf{C}i} = = std(\mathbf{r})\ (diag(\mathbf{J}_{\mathbf{C}i}(\mathbf{J_Q}^\mathbf{T}\mathbf{J_Q})^{-1}\mathbf{J}_{\mathbf{C}i}))^{0.5}$ where $\mathbf{J}_{\mathbf{C}i}$ is a new Jacobian matrix, containing the derivatives of the column *i* of **C** to respect **a** elements at the solution. The same procedure was applied to obtain the asymptotic errors for the columns of **S**, i.e., the estimated intermediate difference spectra, and for the differences between some columns of **S**, i.e., $L - M_1$, $M_2 - M_1$, and $N - M_2$ difference spectra. The error propagation procedure fully takes into account the error correlations in the estimated intrinsic rate constants but should be considered approximate, since it is strictly correct only for linear transformations, and both **C** and **S** are nonlinear functions of the intrinsic rate constant. These standard errors were used to construct 90% confidence intervals for the rate and equilibrium constants, for the intermediates fractions, and for the intermediate difference spectra, as $\pm\ 1.645\sigma$. These confidence intervals

(27) Cameron, D. G.; Moffatt, D. J. *Appl. Spectrosc.* **1987**, *41*, 539–544.
(28) Lórenz-Fonfría, V. A.; Padrós, E. *Spectrochim. Acta A* **2004**, *60*, 2703–2710.
(29) Lórenz-Fonfría, V. A.; Kandori, H. *Appl. Spectrosc.* **2007**, *61*, 428–443.
(30) Shrager, R. I.; Hendler, R. W. *J. Biochem. Biophys. Methods* **1998**, *36*, 157–173.
(31) Chu, M. T. *SIAM Rev.* **1998**, *40*, 1–39.
(32) Johnson, M. L.; Faunt, L. M. *Methods Enzymol.* **1992**, *210*, 1–37.

Table 1. Asymptotic 90% confidence intervals for the estimated intrinsic rate constants, equilibrium constants, and relaxation rate constant of the bR photocycle at 293 K, pH 7, and ~92% relative humidity[a]

	K↔L	L↔M_1	M_1↔M_2	M_2↔N	N↔O	O→BR
k_f^{-1}	6.3−9.8 μs	35−56 μs	170−200 μs	5.0−7.0 ms	2.0−3.0 ms	6.9−8.8 ms
k_b^{-1}	6.4−9.1 μs	290−420 μs	6.6−90 ms	1.6−2.1 ms	7.6−13 ms	∞
K_{eq}	0.7−1.4	5.9−11	36−470	0.28−0.35	3.4−4.9	∞
k_{relax}^{-1}	3.6−4.2 μs	32−48 μs	170−200 μs	1.2−1.6 ms	1.6−2.4 ms	6.9−8.8 ms

[a] k_f, rate constant for the forward transition; k_b, rate constant for the backward transition; K_{eq}, equilibrium constant of the transition, given by k_f/k_b; k_{relax}, relaxation rate constant of the transition, given by $k_f + k_b$. For the O→BR transition k_b was zero by definition.

provide information on how much the solutions obtained may change if the macroscopic rate constant provided by global exponential fitting and the experimental kinetics for the intermediates changed within their observed errors. All the calculations were performed in Matlab version 7 (The Math Works, Natick, MA).

3. Results and Discussion

Deprotonation of the PRG Takes Place between the M Substates. One of the long-standing enigmas in the bR photocycle is the nature of the group releasing the proton to the EC side, the PRG.[6] It has been show that the deprotonation of the PRG is correlated with a peculiar signature in the IR, the *continuum* band.[33] The *continuum* band has been assigned to arise from a delocalized proton, shared either by a cluster of internal water molecules,[33,34] or by two glutamates (Glu204/Glu194).[35] The exact timing of the PRG deprotonation is also uncertain but is often quoted to take place in the L-to-M transition,[36,37] just too early to be directly involved in the *switch* mechanism. Although the kinetics of the transient pH decrease at the EC surface have been thoroughly measured and characterized by covalently linked fluorescein,[38−40] the kinetics dependence on the position of linked dye[40] argues against the total equivalence of the transient pH changes in the EC surface and the kinetics of the PRG deprotonation. The characteristic *continuum* band in the infrared provides finally a selective, and not perturbing internal probe, to test accurately the timing of the PRG deprotonation.

As we have shown before,[22] at earliest times the bR photocycle is dominated by a broad bilobule in the 4000−2500 cm^{-1} region (Figure 2a), which decreases exponentially with time (Figure 2a, Insert). This band originates from a ~0.3 K transient heating of the sample by the actinic laser,[22] with a contribution extending below 2150 cm^{-1} in the form of a positive baseline (Figure, 2a), previously confused with a feature of the photocycle itself.[41] Thus, an attempt to obtain the PRG kinetics directly from the broad *continuum* band happens not to be reliable (Figure 2b, Insert, green line), requiring the subtraction of the transient heat contribution (described in the Supporting Information). The kinetics of the corrected *continuum* band area is presented in Figure 2b (Insert, red lines), and the efficiency of the correction is nicely attested by the flatness of the difference spectra above 2000 cm^{-1} (Figure 2b). The area of the carboxylic band between 1772−1749 cm^{-1} (Figure 2b Insert, blue line) reports selectively the kinetics of the protonation of Asp85,[42] and an unambiguous comparison of the timing of the Asp85 protonation and PRG deprotonation is now possible.

The difference spectra normalized by the Asp85 carboxylic band area reveal that the intensity of the *continuum* band increases with time relative to the Asp85 area (Figure 2c), i.e., Asp85 protonation and PRG deprotonation are not completely synchronous processes. The ratio of the PRG/Asp85 deprotonation/protonation is close to zero before ~10 μs, and then increases, reaching a plateau at ~1 ms, with an inflection point at ~200 μs (Figure 2c, Insert). These results verify that the PRG deprotonation does not take place in the L-to-M transition, but it is slightly delayed relatively to the Asp85 protonation, taking place in between two M substates, as previously suggested.[43] It is possible to get a direct estimate of the relative fractions of the M and N+O intermediates (Figure 2d), and also for the two M substates (Figure 2e): before ($M_{PRG\text{-}H+}$) and after (M_{PRG}) PRG deprotonation (details in the figure legend).

Kinetic Analysis: Transition between the M Substates Is Unidirectional. As a kinetic scheme to analyze the bR photocycle, K ↔ L ↔ M_1 ↔ M_2 ↔ N ↔ O → BR was used which requires the estimation of 11 intrinsic rate constants. This minimum kinetic scheme enjoys ample support in the literature.[5,6,16] Moreover, it is also completely coherent with the kinetic model-free results from singular value decomposition (SVD) and global exponential fitting (G-Exp) presented in Figure 3. SVD shows only five components assignable to a signal (Figure 3b−d), implying that five intermediates (with distinctive spectra/kinetics) are present in the bR photocycle. In turn, G-exp (Figure 3d, red lines) reveals that the total number of intermediates (whether spectrally/kinetically degenerated or not) is at least six. Both results can be brought into agreement if two of the intermediates are spectrally degenerated: e.g., K, L, M_1, M_2, N, and O, with M_1 and M_2 substates spectra nearly identical within the noise.

Having a kinetic scheme, we need to estimate the intrinsic rate constants. A consistent kinetic model describing optimally the time-resolved data should guaranteed that the minus eigenvalues of the kinetic matrix agree with the rate constants provided by global exponential fitting.[20,44] On the basis of this simple fact, we have developed an innovative and robust approach for the kinetic analysis of photocycles. Briefly, given a kinetic scheme (e.g, A↔B→C), the intrinsic rate constants (e.g., $k_{A\to B}$, $k_{B\to A}$, and $k_{B\to A}$) are iteratively adjusted until the eigenvalues of the corresponding kinetic matrix agree with the macroscopic rate constants obtained by a global exponential

(33) Garczarek, F.; Brown, L. S.; Lanyi, J. K.; Gerwert, K. *Proc. Natl. Acad. Sci. U.S.A.* **2005**, *102*, 3633–3638.
(34) Mathias, G.; Marx, D. *Proc. Natl. Acad. Sci. U.S.A.* **2007**, *104*, 6980–6985.
(35) Phatak, P.; Ghosh, N.; Yu, H.; Cui, Q.; Elstner, M. *Proc. Natl. Acad. Sci. U.S.A.* **2008**, *105*, 19672–19677.
(36) Garczarek, F.; Gerwert, K. *Nature (London)* **2006**, *439*, 109–112.
(37) Mak-Jurkauskas, M. L.; Bajaj, V. S.; Hornstein, M. K.; Belenky, M.; Griffin, R. G.; Herzfeld, J. *Proc. Natl. Acad. Sci. U.S.A.* **2008**, *105*, 883–888.
(38) Heberle, J.; Dencher, N. A. *FEBS Lett.* **1990**, *277*, 277–280.
(39) Cao, Y.; Brown, L. S.; Sasaki, J.; Maeda, A.; Needleman, R.; Lanyi, J. K. *Biophys. J.* **1995**, *68*, 1518–1530.
(40) Alexiev, U.; Marti, T.; Heyn, M. P.; Khorana, H. G.; Scherrer, P. *Biochemistry* **1994**, *33*, 13693–13699.
(41) Wang, J.; El-Sayed, M. A. *Biophys. J.* **2001**, *80*, 961–971.

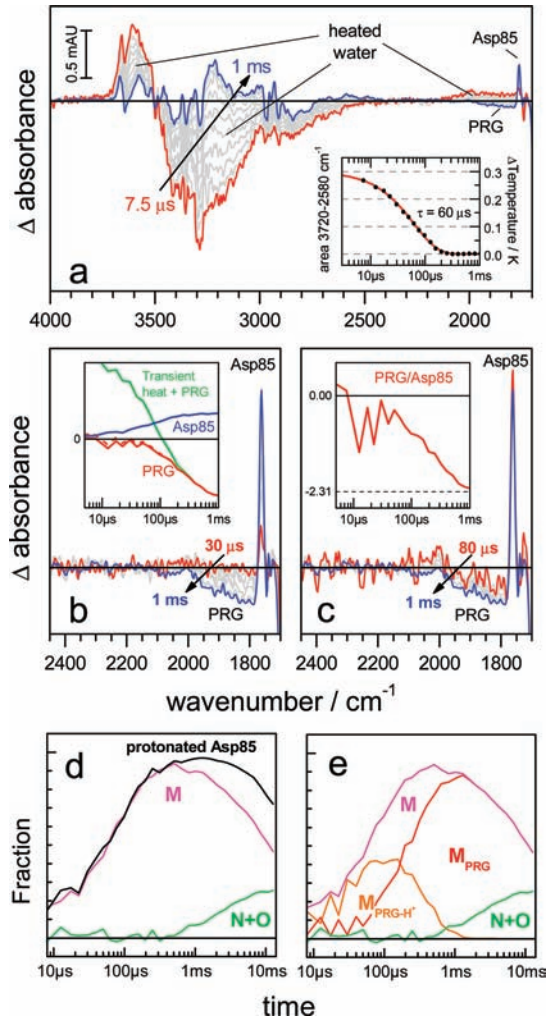

Figure 2. Relation between the kinetics of Asp85 protonation and PRG deprotonation, and spectroscopic estimation of the kinetics of two M substates. (a) Time-resolved FTIR difference spectra for the bR photocycle. (Insert) Kinetics of the transient heat dissipation (black dots), fitted to a single exponential decay (red line). (b) Time-resolved FTIR difference spectra corrected for the transient heat. (Insert) Kinetics of the Asp85 carboxylic area from 1772−1749 cm^{-1} (blue), and PRG area from 2000−1800 cm^{-1} before (green) and after (red, dashed) the transient heat correction. Small distortions introduced by the transient heat correction were corrected as described in the Supporting Information (red, continuous). (c) Same as (b) but normalized by the Asp85 area. (Insert) Time evolution of the PRG/Asp85 ratio. The dashed line marks the extrapolated maximum ratio. (d) The kinetics of the area between 1772−1749 cm^{-1} gives the fraction of intermediates with a protonated Asp85, M+N+O (black line), while the area between 1774−1554 cm^{-1} gives the kinetics of the protonated Asp85 in the M intermediate (pink line);[42] after scaling their subtraction the kinetics of Asp85 in the N+O intermediates (green line) are obtained. (e) Identical to (d), but from the ratio in (c, Insert) the fractions of the M intermediate before and after the PRG deprotonation were estimated.

fitting within experimental error. Any remaining ambiguity can be removed/attenuated by adding a secondary convex goal (as described in Methods). In the present application we used as a secondary goal the approximate description of the kinetics of some IR bands roughly selective for the different intermediates (see Supporting Information, Figure S1).

Figure 4a displays the estimated intrinsic time constants for the bR photocycle, and Table 1 provides their confidence intervals, together with the confidence intervals for the equilibrium constants and the relaxation constants for the different steps of the bR photocycle under our experimental conditions. According to the obtained solution all the steps are relatively

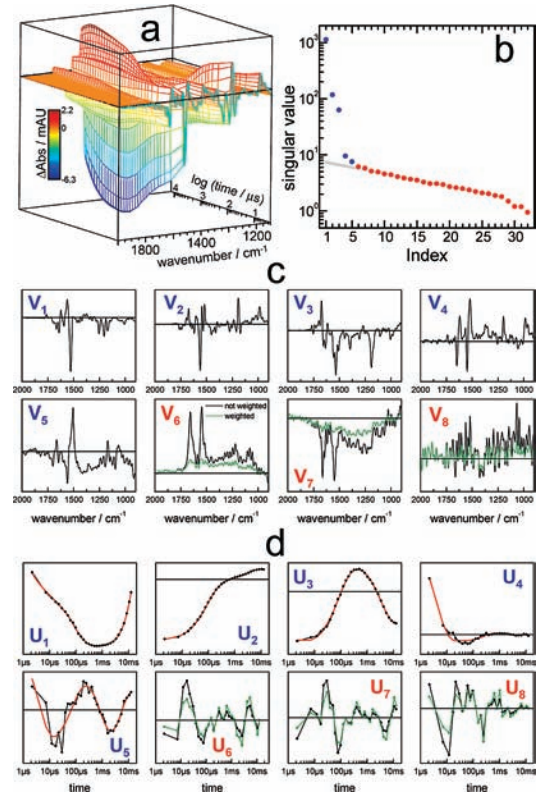

Figure 3. Singular value decomposition and global exponential analysis of the time-resolved data. (a) Three-dimensional (3D) plot of the data analyzed (from 2000−900 cm^{-1} and 2.5 μs−13 ms). For displaying purposes the data corresponding to the data reconstructed from the first five singular value components are plotted instead of the raw data. (b) Singular values, assigned either to signal (blue) or noise (red) components. The gray line is an exponential fit to the 8−28 singular values. (c) Raw abstract spectra associated to the first eight singular values (black), and for the components assigned to noise after being weighted according to the noise standard deviation (green). (d) Raw abstract time-traces (connected black dots), and after weighting for the noise standard deviation (connected green dots). Best fit by global exponential fitting using six exponentials (red line), with time constants: 3.8 μs, 78 μs, 220 μs, 920 μs, 4.6 ms, and 26 ms.

close to equilibrium, with a $K_{eq} \approx 0.3-8$ (see Table 1). The exceptions are the ground-state recovery, O-to-BR, which was unidirectional by model definition to make BR the resting state, and the transition between the M substates, with an equilibrium constant ~100. Indeed, forcing the M_1 to M_2 transition to be completely unidirectional provided almost identical results (Supporting Information, Figure S3). In contrast, when the rest of transitions were forced to be unidirectional, the obtained solutions showed unusual intermediate difference spectra, and/or high deviations from the expected intermediates fractions (Supporting Information, Figures S3, S4). Therefore, the transition between two M substates (M_1-to-M_2) is the only unidirectional step in the photocycle besides the O-to-BR transition.[16] The estimated fractions for the bR intermediates during the photocycle are displayed in Figure 4b (continuous lines), with their corresponding confidence intervals (dashed lines).

Infrared Difference Spectra for the bR Intermediates and the M Substates. Once a kinetic model was obtained, we calculated the infrared difference spectra for all the photocycle

(42) Perálvarez-Marín, A.; Lórenz-Fonfría, V. A.; Bourdelande, J.-L.; Querol, E.; Kandori, H.; Padrós, E. *J. Mol. Biol.* **2007**, *368*, 666–676.
(43) Zimányi, L.; Váró, G.; Chang, M.; Ni, B.; Needleman, R.; Lanyi, J. K. *Biochemistry* **1992**, *31*, 8535–8543.
(44) Shrager, R. I.; Hendler, R. W. *J. Phys. Chem. B* **2003**, *107*, 1708–1713.

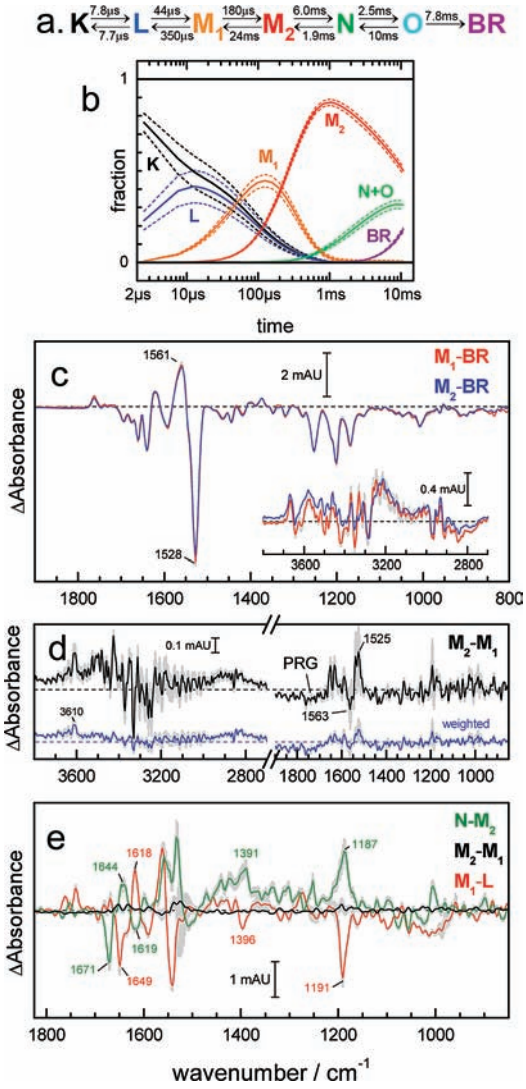

Figure 4. Kinetic analysis of the photocycle and characterization of the transition between M substates. (a) Kinetic scheme and the estimated intrinsic time constants. The reciprocal of the negative eigenvalues of this kinetic model are ~3.7 μs, 66 μs, 250 μs, 920 μs, 4.7 ms, and 27 ms, in good agreement with the time constants determined by global exponential fitting (Figure 3d). Confidence intervals for the estimated intrinsic rate constant are provided in Table 1. (b) Corresponding intermediate fractions derived from the kinetic model (continuous lines), with their estimated confidence intervals (dashed lines). (c) M_1 − BR and M_2 − BR infrared spectra obtained from the experimental data and the estimated intermediate fractions in (b). (Insert) The X−H stretching region. (d) M_2 − M_1 infrared spectrum (black line). For a better appreciation of the noise-induced features, the M_2-M_1 difference spectrum was weighted by the estimated noise standard deviation dependence on wavenumber (blue). (e) Comparison of the estimated M_1-L, M_2-M_1 and N-M_2 difference spectra, with an offset at 1850 cm^{-1}. In (c−e) the vertical light-gray lines indicate confidence intervals for the spectra, obtained as described in Methods.

intermediates with their confidence intervals (Supporting Information, Figure S5). The obtained spectra closely resemble previous estimates,[45−47] except for the O − BR difference spectrum (see Supporting Information, Figure S5 legend for possible explanations for this discrepancy). We have observed that by using slightly altered kinetic schemes (e.g., removing a back-reaction) the obtained difference spectra provided by our analysis were nearly identical for all the intermediates not directly implicated in the alteration (see Supporting Information, Figures S3c, S4c), i.e., the difference spectra estimated by our method are reasonably robust to changes in the kinetic scheme used in the analysis.

Figure 4c shows the M_1 − BR and M_2 − BR difference spectra with their confidence intervals, indicated by gray vertical lines. In the 1850−800 cm^{-1} region the IR difference spectra reports changes in the protein backbone, retinal, SB and amino acid side chains.[18] Both the M_1 − BR and M_2 − BR spectra agree with previous estimates of the M − BR spectrum in this region.[45−48] In the insert, we show the X−H stretching region, contributed mostly by the changes in the H-bonding of N−H and O−H groups, including those of the internal water molecules.[49] The spectra are astonishingly similar in both regions (note the difference in scale). In particular, the retinal fingerprint region (1300–1100 cm^{-1}) totally agrees between the M substates. Having a deprotonated SB, the M intermediate is the only intermediate with a negligible contribution in the retinal fingerprint region,[18] and so changes in this region between M substates are not possible for genuine M substates. This is a simple but crucial spectroscopic confirmation that the *bona fide* M substates are resolved in the present paper, with negligible contributions from other intermediates, validating in turn the success of the kinetic analysis. Further support comes from the visual agreement of the retinal fingerprint region with previous double-flash experiments designed to obtain a pure M − BR difference spectrum.[48] Additionally, in spite of the differences in sample and acquisition conditions, when the retinal fingerprint region was fitted to the intermediate spectra obtained by Zscherp and Heberle[46] (kindly provided by Prof. Heberle) our M_1 − BR and M_2 − BR difference spectra were estimated to correspond to ~95% of M, with only a ~5% contribution of L and N intermediates, respectively.

Spectral Signatures of the Transition between M Substates. The remarkable similarity of the M substates is more sensibly attested to in the M_2 − M_1 difference spectrum (Figure 4d, black line, with confidence interval displayed in gray vertical lines). A negative broad feature is observed above 1700 cm^{-1} in the M_2 − M_1 difference spectrum (Figure 4d). This broadband can be assigned to the *continuum* band, in coherence with the results showing that PRG deprotonation takes place between two M substates (Figure 2). The intensity of this negative broad feature is slightly lower than 0.1 mAU, in agreement with the maximum intensity of the *continuum* band observed in samples at 92% relative humidty,[22] although for unknown reasons 3 times less intense than the *continuum* band maximum intensity observed in fully hydrated samples.[50]

Other significant features in the M_2 − M_1 difference spectrum are less obvious. Most apparent peaks, like the positive/negative peaks at 1525/1563 cm^{-1}, show intensities within the confidence interval, and cannot be rendered as significant. To aid further the visualization of significant features, the M_2 − M_1 difference spectrum was weighted by the noise standard dependence on wavenumber (Figure 4d, blue line). After this weighting the noise amplitude becomes constant with the wavenumber. A positive baseline around 3100−2700 cm^{-1} and a narrow band

(45) Heβling, B.; Souvignier, G.; Gerwert, K. *Biophys. J.* **1993**, *65*, 1929–1941.
(46) Zscherp, C.; Heberle, J. *J. Phys. Chem. B* **1997**, *101*, 10542–10547.
(47) Rödig, C.; Chizhov, I.; Weidlich, O.; Siebert, F. *Biophys. J.* **1999**, *76*, 2687–2701.
(48) Hessling, B.; Herbst, J.; Rammelsberg, R.; Gerwert, K. *Biophys. J.* **1997**, *73*, 2071–2080.
(49) Kandori, H. *Biochim. Biophys. Acta* **2000**, *1460*, 177–191.
(50) Rammelsberg, R.; Huhn, G.; Lübben, M.; Gerwert, K. *Biochemistry* **1998**, *37*, 5001–5009.

at 3610 cm^{-1} are observed, which could be assigned to the formation of strong and weak H-bonds in the internal waters during the M_1-to-M_2 transition. Further verification of the assignment of these bands to water molecules by using $H_2{}^{18}O$ was unfeasible by the high level of the noise in the resulting $M_2 - M_1$ difference spectrum (not shown).

Protein Structural Changes in the Transition between the M Substates. The amide I region of the $N - M_2$ difference spectrum is dominated by a negative band at 1671 cm^{-1} (Figure 4e, green). A positive band at 1660 cm^{-1}, usually observed only at high sample tilt angles,[51] become resolved in our $N - M_2$ spectrum only after band-narrowing (Supporting Information Figure S6). From the 1671 and 1660 cm^{-1} band areas relative to the amide I area in the absolute spectrum (not shown), and assuming them to arise solely from tilt changes in transmembrane helices, we roughly estimated a ~5° decrease and a ~1° increase in the tilt of two full transmembrane helices in the M_2-to-N transition (details of the estimation available in the Supporting Information). The sign and estimated tilt change of these two bands is coherent with previous diffraction studies, reporting an inward and outward helix movement for the helices G and F in the M-to-N transition.[52]

Comparing the intense $N - M_2$ difference spectrum with the flat $M_2 - M_1$ difference spectrum (Figure 4e, green vs black line), we can clearly deduce the absence of significant conformation/orientation changes in the protein backbone during the *switch* step. The $M_2 - M_1$ difference spectrum does not show significant bands in amide I (1700−1610 cm^{-1}), nor in the amide II region (1580−1510 cm^{-1}). Two peaks are observed at 1525 (+), 1563 (−) cm^{-1} but are within the error (Figure 4d).

Changes in the Retinal and the SB in the Transition between the M Substates. The retinal C−C stretching vibrations, known as the retinal fingerprint, are exceptionally sensitive to the retinal conformation.[18,53] However, in the infrared, the intensity of these bands decreases strongly when the SB is unprotonated, becoming silent to the retinal conformation in the M intermediate.[18] Nevertheless, in the $M_2 - M_1$ difference spectrum the absence of any bands at the region of the retinal HOOP vibrations (1000−900 cm^{-1}), sensitive to the retinal curvature,[18] indicates that retinal planarity does not change in the M_1-to-M_2 transition.

Resonance Raman studies have assigned the C=N stretching for the deprotonated SB (M intermediate) at 1621 cm^{-1}, and for the protonated SB in the L and N intermediates at 1645 cm^{-1}.[53,54] In agreement, the L-to-M_1 transition shows bands at 1649 (−) and 1618 (+) cm^{-1} (Figure 4e, red line), reporting for the deprotonation of the SB, together with the bands at 1396 (−) and 1191 (−) cm^{-1}, assigned to the SB N−H bend and retinal C−C stretching, respectively.[53] Coherently, upon SB reprotonation in the M_2-to-N transition, equivalent bands appear at 1646 (+), 1619 (−), 1391 (+), and 1187 (+) cm^{-1} (Figure 4e, green line). The absence of a band at around ~1618 cm^{-1} in the M_2-M_1 spectrum (Figure 4b, black line), suggests that the environment/orientation of the deprotonated SB does not change during the *switch*, or at least not sufficiently.

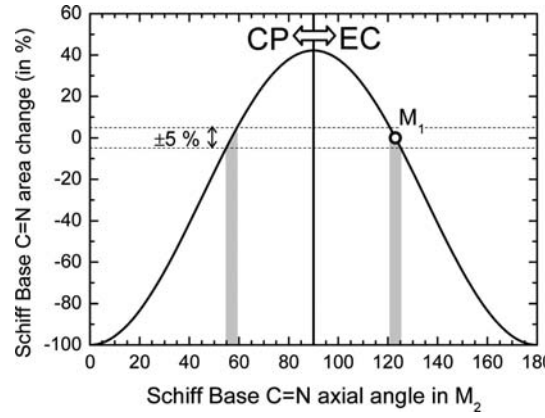

Figure 5. Possible SB orientation change between M substates deduced from IR spectroscopy. Expected relative area of the unprotonated Schiff Base (SB) band at 1618 cm^{-1} in the M_2-M_1 difference spectrum as a function of the SB C=N orientation in the M_2 substate. Assuming that a 5% area change (or lower) could go undetected, the possible orientation of the SB C=N in the M_2 substate is shadowed in light gray. The vertical continuous black line separates a SB with a cytoplasmic (CP) and extracellular (EC) orientation. The orientation of the SB in the M_1 substate is given (open circle) following the crystallographic structure 1m0m.[55] This same figure can be alternatively interpreted as giving possible SB orientations in M_1 given the SB orientation in M_2.

We considered the possibility of changes in the orientation of the SB more quantitatively. Taking the angle between the C=N bond and the membrane normal to be 123.3° in M_1 (from the M structure at the higher available resolution, pdb 1m0m[55]), we calculated from the absence of any band ~1618 cm^{-1} that the SB angle in M_2 is either between 120.8−125.2° or between 54.8−59.2°, where angles higher/lower than 90° correspond to an EC/CP orientation of the SB, respectively (see Figure 5, and the Supporting Information for further details). These estimates were obtained, considering that a 5% change in the intensity of the C=N vibration should be observable in the $M_2 - M_1$ difference spectrum. Given the symmetry of the problem, Figure 5 can also be interpreted as giving possible SB orientations in M_1 for a SB orientation in M_2 of 123.3°. This means that whether the pdb 1m0m structure corresponds to a M_1 or a M_2 intermediate, we can conclude from our infrared data that the SB orientation does not change in the *switch*, ±(−2.5° − +1.9°), or else, it reorientates symmetrically between the EC−CP (or CP−EC) domains, ±(64.1° − 68.5°). An equivalent analysis was performed using the SB orientation for the other four structures of the M intermediate (1p8h,[56] 1kg8,[57] 1iw9,[58] and 1cwq[59]), and the results are available in the Supporting Information, Figure S7. In all cases, our IR data are consistent both with the absence of changes in the SB orientation between M substates (whether initially EC or CP), or with a symmetrical EC-to-CP (or CP-to-EC) reorientation.

4. General Discussion

In the present work we have compared the kinetics of the *continuum* band (signature of the PRG deprotonation) and the

(51) Kandori, H. *J. Am. Chem. Soc.* **1998**, *120*, 4546–4547.
(52) Oka, T.; Yagi, N.; Fujisawa, T.; Kamikubo, H.; Tokunaga, F.; Kataoka, M. *Proc. Natl. Acad. Sci. U.S.A.* **2000**, *97*, 14278–14282.
(53) Althaus, T.; Eisfield, W.; Lohrmann, R.; Stockburger, M. *Isr. J. Chem.* **1995**, *35*, 227–251.
(54) Smith, S. O.; Lugtenburg, J.; Mathies, R. A. *J. Membr. Biol.* **1985**, *85*, 95–109.
(55) Lanyi, J.; Schobert, B. *J. Mol. Biol.* **2002**, *321*, 727–737.
(56) Schobert, B.; Brown, L. S.; Lanyi, J. K. *J. Mol. Biol.* **2003**, *330*, 553–570.
(57) Facciotti, M. T.; Rouhani, S.; Burkard, F. T.; Betancourt, F. M.; Downing, K. H.; Rose, R. B.; McDermott, G.; Glaeser, R. M. *Biophys. J.* **2001**, *81*, 3442–3455.
(58) Takeda, K.; Matsui, Y.; Kamiya, N.; Adachi, S.; Okumura, H.; Kouyama, T. *J. Mol. Biol.* **2004**, *341*, 1023–1037.
(59) Sass, H. J.; Buldt, G.; Gessenich, R.; Hehn, D.; Neff, D.; Schlesinger, R.; Berendzen, J.; Ormos, P. *Nature (London)* **2000**, *406*, 649–653.

kinetics of Asp85 protonation (signature of the SB deprotonation) to confirm whether these two proton transfers are simultaneous (Figure 2). We have also presented a kinetic analysis of the bR photocycle, focused in the spectral changes associated with the transition between two M substates (Figure 4), the step where the SB proton affinity/accessibility is expected to switch from the EC to the CP domain.

The first part of the Results (Figure 2b,c) shows that the PRG deprotonation is delayed to respect Asp85 protonation. This observation calls for two M substates, before and after PRG deprotonation. Additionally, this finding allowed us to roughly estimate, without any kinetic analysis, their relative fractions with respect to time (Figure 2d,e). We should stress than the spectral contribution of the transient heat of the sample was subtracted before obtaining the kinetics of the *continuum* band, and therefore its kinetics before ~200 μs could be affected in case of an imperfect subtraction. However, the differences in the *continuum* band and Asp85 kinetics persisted above 200 μs (Figure, 2c insert), where the transient heat is totally dissipated (Figure 2a insert), confirming that independently of the success of the transient heat subtraction procedure we can conclude that the PRG deprotonation is delayed with respect to Asp85 protonation.

The results of the posterior kinetic analysis support previous evidence for a unidirectional transition between two M substates.[16] The rest of the transitions appear to be nearly at equilibrium, except for the unidirectional recovery of BR from the O intermediate (Figure 4a and Table 1). The kinetic analysis also revealed that the transition between the two M substates is associated with very few and small spectroscopic changes in the infrared, basically reduced to the negative *continuum* band associated to the PRG deprotonation (Figure 4d).

Critical Assessment of the Successful Resolution of M Substates. The somehow unexpected high spectral similarity of the M substates deserves some comments and clarifications about the possible failure of the performed kinetic analysis. One way the resolution of the M substates could fail is by an unsuccessful complete kinetic resolution of the M_1 and M_2 intermediates from their closer temporal neighbors: the L and N intermediates. However, this condition could be easily diagnosed by BR−L, N−BR, or N−L contributions in the M_2-M_1 spectrum, which are not observed in Figure 4e. Actually, the fact that our M_2-M_1 spectrum shows almost no bands is incompatible with contaminations from L and/or N intermediates, or even K or O intermediates.

The kinetic analysis may also have failed by splitting one single intermediate into two intermediates, i.e., our M_1−BR and M_2−BR spectra could correspond to the same identical M intermediate, erroneously resolved into two during the analysis. However, several evidences suggest that the two M substates resolved here are truly two different states in the bR photocycle. (a) As Varo and Lanyi reported,[60] to describe the bR photocycle we need at least two M substates, one M equilibrated with L and another M equilibrated with N. Otherwise, L intermediates keep equilibrated with the N intermediate, and the experimental intermediate fractions cannot be reproduced. (b) Results from global exponential fitting (Figure 3) imply that there are at least six intermediates in the photocycle. This means that for at least one standard intermediate (e.g., M) there should be two substates (e.g., M_1 and M_2). (c) The results of SVD and global exponential fitting (Figure 3), independent of any specific kinetic model, suggest that two intermediates have nearly degenerated spectra, in coherence with the observed high spectral similitude of the M_1 and M_2 intermediates. (d) The results in Figure 2 show that the PRG deprotonates after Asp85 protonation, evidencing that the PRG deprotonation occurs between two M substates, i.e., the M_1 and M_2 substates resolved here are similar but not identical states.

Involvement of Protein Backbone Changes in the Switch. Diffraction studies on purple membranes have revealed clear changes in the tilt of the transmembrane F and G helices during the photocycle,[7,8,61] interpreted as a transient opening of the CP domain, from where a proton becomes captured before bR recovery to the ground state. These changes have been assigned to occur in between M substates,[7,11] i.e., during the *switch* step, leading to a model with two alternate conformations: an outward-facing EC conformation (for BR, K, L, and M_1) and an inward-facing CP conformation (for M_2, N and O).[11] The similitude with the structural changes proposed to occur in some secondary transporters is evident, where alternative CP−EC access of the substrate binding-site is proposed to occur by switching between an inward-facing (CP) to an outward-facing (EC) conformation.[62] If correct, this would support a conceptually common *switch* mechanism for both primary and secondary transporters.

The data presented here gives strong evidence for the lack of protein structural changes between the M substates, also excluding changes in the helix tilting (Figure 4c,d). This supports previous time-resolved EPR and FT-IR studies, reporting either small[47] or negligible[48,63] structural changes between the M substates. Changes in the tilt of some helices are observed, but not until the M_2-to-N transition (Figure 4e). Incidentally, the estimated equilibrium constant for this transition suggests that these structural changes are thermodynamically slightly disfavored (see Table 1). The tilt of the helices, even if important in the proton transport mechanism, is probably not involved in the *switch* mechanism that ensures proton-pump vectoriality in bR.

Previous results from time-resolved diffractions experiments on the wild-type photocycle can be satisfactorily explained by an insufficient account of the temporal overlap of intermediates. We have reanalyzed recent microsecond time-resolved X-ray diffraction data of Oka et al. at 7 Å and 6 μs resolution,[64] confirming that the main structural changes in the bR photocycle do occur in the M_2-to-N transition. Figure 6a reproduces the second abstract time-trace for the time-resolved data of Oka et al. (filled circles with connected lines). Roughly, it corresponds to the scattering changes during the photocycle relative to the ground state. We assumed that the intermediate fractions in our experimental conditions are translatable to their experimental conditions (see Supporting Information and Figure S8 for evidence that supports this assumption). We fitted our estimated intermediate fractions to their scattering data (Figure 6a red dashed line). The fit is relatively good, although significant deviations after 20 ms are evident. Our interpretation of Oka et al. data is summarized in Figure 6b. In the M_2-to-N transition we have the main structural change, accounting for ~63% of

(60) Váró, G.; Lanyi, J. K. *Biochemistry* **1991**, *30*, 5008–5015.
(61) Subramaniam, S.; Gerstein, M.; Oesterhelt, D.; Henderson, R. *EMBO J.* **1993**, *12*, 1–8.
(62) Law, C. J.; Maloney, P. C.; Wang, D. N. *Annu. Rev. Microbiol.* **2008**, *62*, 289–305.
(63) Steinhoff, H. J.; Mollaaghababa, R.; Altenbach, C.; Hideg, K.; Krebs, M.; Khorana, H. G.; Hubbell, W. L. *Science* **1994**, *266*, 105–107.
(64) Oka, T.; Inoue, K.; Kataoka, M.; Yagi, N. *Biophys. J.* **2005**, *88*, 436–442.

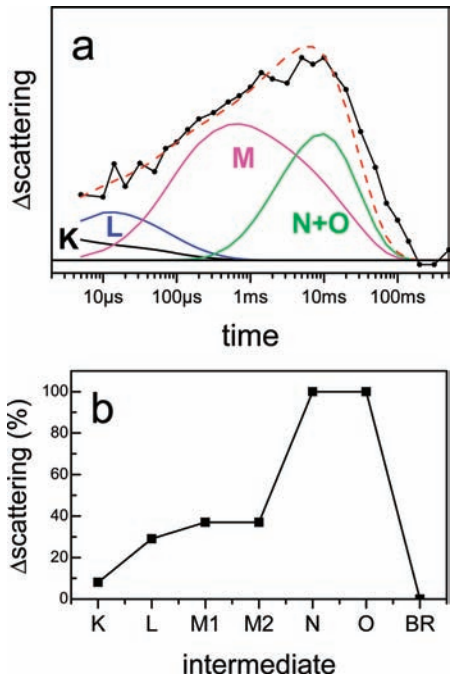

Figure 6. Re-analysis of time-resolved X-ray scattering data, showing where the structural changes take place in the bR photocycle. (a) The second SVD abstract time-trace obtained from the integrated time-resolved diffraction patter reproduced from Oka et al. [64] (connected black circles). The intermediate fractions obtained for our experimental conditions were scaled to fit the diffraction time-trace. The fit is shown in red dashed line. (b) Estimated relative diffraction change for each intermediate, calculated from the scaling factor of the intermediates fractions used to fit the data in (a).

the scattering change. The estimates presented in Figure 6b should be considered approximate and taken with prudence, but these nicely illustrate the fact that X-ray scattering results can be explained by structural changes taking place mainly in the M_2-to-N transition, with a structural silent transition between the M substates.

We should finally note that in mutants lacking a CP proton donor (e.g., Asp96Asn) an atypical M intermediate appears, M_N, structurally similar to the N intermediate but with an unprotonated SB.[65] Under these conditions the transition between two M substates, i.e., M_2-to-M_N, is reasonably expected to be associated with conformational changes (as the normal M_2-to-N transition), but unlikely to be involved in the *switch* mechanism.

Involvement of Changes in the Retinal and/or SB in the Switch. A change in the retinal curvature was proposed as one of the possible mechanism for the *switch*.[11] However, our $M_2 - M_1$ difference spectrum does not show bands in the HOOP region of the (Figure 4d), suggesting absence of changes in the retinal planarity between the M substates, in agreement with previous resonance Raman data.[53,54]

An attractive mechanism for the *switch* mechanism is the SB reorientation from Asp85 to Asp96.[6,10] This could be accomplished if during the M lifetime the twisted 13-*cis*-15-*anti* retinal relax through rotations around the $C_{14}-C_{15}$ and/or $C_{15}=NZ$ bonds.[6] Our results suggest that the SB orientation relative to the membrane normal may not change by more than $\pm 5°$ between the M substates (see Figure 5 and Supporting Figure S7). This does not reject SB reorientation between M substates, but if the reorientation must take place, the SB orientation in M_2 should be nearly the mirror image of its orientation in M_1. Having a SB pointing to opposite domains, perceptible changes in the retinal conformation should be expected. However, low-temperature NMR studies did not detect any significant changes in the $HC_{14}-C_{15}H$ retinal dihedral angle between trapped M substates.[10] More significantly, time-resolved resonance Raman spectroscopy experiments, where the M intermediate was selectively probed by its distinct blue shift in the UV−vis, did not revealed obvious differences in the retinal fingerprint region from 20 μs until >5 ms,[66] convincingly arguing against substantial retinal conformational changes and SB reorientation between M substates.

We should note that two X-ray crystallographic structures of the wild type M intermediate at a resolution ≤ 1.6 Å (pdb 1m0m[55] and 1p8h[56]) show electron densities clearly corresponding to a SB with an EC orientation, while three other structures at a resolution ≥ 2 Å (pdb 1kg8,[57] 1cwq,[59] and 1iw9[58]) were modeled with a SB with a CP orientation, possible evidence for SB reorientation between M substates. However, we should keep in mind the controversial results about the SB orientation in the L[67−69] and in the K[70,71] intermediates obtained by different groups, suggesting difficulties of X-ray crystallography to unambiguously reveal the orientation of the SB. In a recent work the problem of determining SB orientation for a bR intermediate by X-ray crystallography was addressed in detail.[72] In spite of the high resolution (up to 1.53 Å) and high intermediate occupancy (~60%), during the refinement, both an EC and a CP orientation for the SB were equally compatible with the diffraction data, confirming the limitations of X-ray crystallography to prove a well-defined and biasless SB orientation.

Given the little direct experimental evidence in favor, we should tentatively conclude that the SB does not change its orientation between the M substates, and its reorientation is therefore unlikely to be involved in the *switch* mechanism of bR. Assuming an EC orientation in M_1, SB reorientation does not probably occur until the M_2-to-N transition. However, it cannot be excluded that the SB adopts a CP orientation already in the L intermediate, or even earlier, as several theoretical works convincingly argue.[73,74]

PRG Deprotonation and the Switch Unidirectionality. The presence of the *continuum*-like band in the $M_2 - M_1$ spectrum (Figure 4d) and especially the detailed comparison of the *continuum* band and Asp85 kinetics (Figure 2) confirm that deprotonation of the PRG occurs between two M substates. Since the *continuum* band is absent in the M intermediate obtained at 230 K,[22] we can conclude that the deprotonation of

(65) Sasaki, J.; Shichida, Y.; Lanyi, J. K.; Maeda, A. *J. Biol. Chem.* **1992**, *267*, 20782–20786.
(66) Ames, J. B.; Mathies, R. A. *Biochemistry* **1990**, *29*, 7181–7190.
(67) Kouyama, T.; Nishikawa, T.; Tokuhisa, T.; Okumura, H. *J. Mol. Biol.* **2004**, *335*, 531–546.
(68) Edman, K.; Royant, A.; Larsson, G.; Jacobson, F.; Taylor, T.; van der Spoel, D.; Landau, E. M.; Pebay-Peyroula, E.; Neutze, R. *J. Biol. Chem.* **2004**, *279*, 2147–2158.
(69) Lanyi, J. K. *Biochim. Biophys. Acta* **2004**, *1658*, 14–22.
(70) Edman, K.; Nollert, P.; Royant, A.; Belrhali, H.; Pebay-Peyroula, E.; Hajdu, J.; Neutze, R.; Landau, E. M. *Nature (London)* **1999**, *401*, 822–826.
(71) Schobert, B.; Cupp-Vickery, J.; Hornak, V.; Smith, S.; Lanyi, J. *J. Mol. Biol.* **2002**, *321*, 715–726.
(72) Lanyi, J. K.; Schobert, B. *J. Mol. Biol.* **2007**, *365*, 1379–1392.
(73) Bondar, A. N.; Elstner, M.; Suhai, S.; Smith, J. C.; Fischer, S. *Structure* **2004**, *12*, 1281–1288.
(74) Hayashi, S.; Tajkhorshid, E.; Schulten, K. *Biophys. J.* **2002**, *83*, 1281–1297.

the PRG requires appropriate protein/water dynamics, as supported by the fact that the M_1-to-M_2 transition is also inhibited at low hydration.[23] This dynamical requirement would agree with recent MD simulations and a time-resolved FT-IR experiment suggesting that the proton release from the PRG requires the opening of a molecular "valve" or "gate", sealed by a H-bond between Ser193 and Glu204.[75] The opening of this hypothetical valve as a condition for the PRG deprotonation would be in agreement with our results inasmuch as it would involve few structural changes, subtle enough to be silent in the infrared $M_2 - M_1$ difference spectrum.

It was reported that as the pH approaches the pK_a of the PRG in the M intermediate, the unidirectional character of the M_1-to-M_2 transition disappears, with an L/M equilibrium maintained through the photocycle,[43] with a substantial population of pre-*switch* intermediates (K, L, M_1) present until the end of the photocycle.[43,76] Taking this information into account, the deprotonation of the PRG seems the most likely driving force behind the observed unidirectionality of the M_1-to-M_2 transition (Figure 4a and Table 1). Interestingly, the full recovery of BR from the O intermediate, essential to complete the transport cycle, involves the PRG reprotonation from Asp85,[6] i.e., the deprotonation/protonation of the PRG seems to be involved in the two unidirectional steps of the bR photocycle.

Unidirectional deprotonation of the PRG in the M_1-to-M_2 transition could play an essential role in the effective coupling of the photon absorption and the proton pumping. It will decrease the lifespan of pre-*switch* intermediates, and thus it will decrease the probability of their unproductive but possible relaxation to BR.[77] Indeed, at moderate hydration (r.h. 90−70%), where the transition from M_1 to M_2 is slowed down, unproductive ground-state recovery from the M_1 intermediate occurs.[23]

The *Switch* Mechanism. The results presented in this work reasonably discard protein backbone or retinal/SB changes between the M substates and, consequently, their involvement in the *switch* mechanism. Deprotonation of the PRG *does* occur in the transition between M substates, and it seems to be tightly linked to the unidirectional character of the *switch*. But what constitutes the core of the *switch* mechanism?

We believe that deprotonation of the PRG is not only the driving force for the unidirectional *switch* but is also its main constituent. In the M_1 intermediate the SB will be able to recover its proton from Asp85 and return temporarily to the L intermediate state, the ratio between M_1/L being ∼8 (Table 1). Unidirectional deprotonation of the PRG in the M_1-to-M_2 transition will lead to a $\sim 10^5$ times increase of the proton affinity of Asp85.[14] The pK_a coupling between the PRG and Asp85 is possibly transmitted through a network of hydrogen bonds connecting them in the ground state (Figure 1), but the detail mechanism of coupling is not resolved here. Once PRG deprotonation takes place, the proton back-flow from Asp85 to the SB (M_2-to-M_1-to-L back-reaction) will be kinetically slow and thermodynamically unfavorable, and Asp85 will effectively retain the proton from the SB. The SB will be forced to remain unprotonated until a CP proton donor becomes available, ensuring a CP-to-EC vectorial proton transport. This *switch* mechanism will be achieved without or with few perceptible changes in the UV−vis, Raman, and IR spectra and will be functional in the pH range given by the pK_a of the PRG in the BR and the M_1 states, i.e., between ∼9.4 and ∼4.7.[14,78] Actually, bR function as a proton pump is optimal at pH 7.5−6 and substantially decreases at pH values above ∼8.5 or below ∼4.5.[79−81]

We briefly consider here the possibility that the *switch* could involve more than one mechanism. One possible secondary mechanism, coherent with our experimental results, is the involvement of the internal water molecules located around the SB. These water molecules are likely to mediate the reversible proton transfer from the SB to Asp85 in the L↔M_1 transition, and therefore it seems mechanistically conceivable that small rearrangements in their H-bonds in the M_1-to-M_2 transition could raise the barrier and slow down the rate for the back-reprotonation of the SB from Asp85.[12] Actually, changes in the H-bond strength of internal water molecules during the M intermediate, in the form of a broad positive baseline change, have been reported recently.[36] A similar broad positive baseline is also observed in our $M_2 - M_1$ difference spectrum, although its assignment to internal waters around the SB region can be, at present, only tentative.

5. Conclusions

The results presented in the present contribution favor an affinity-based over an accessibility-based *switch* mechanism for bR. The affinity *switch* of the SB is provided by the unidirectional deprotonation of the PRG coupled with an increase of the proton affinity of Asp85. This mechanism is supported by recent theoretical studies showing that coupled proton affinity changes alone, i.e., without structural EC−CP accessibility changes, can sustain vectorial proton pumping in bR.[82,83]

In spite of not being a prototype transporter, equally subtle *switch* mechanisms, as those revealed here for bR, could also exist in other active transporters. Nevertheless, their detection could be difficult, being hidden under more prominent protein conformational changes partially overlapping in time, as it is the case of bR. As shown here, time-resolved studies combined with an appropriate account for the temporal overlap of intermediates is a prerequisite for the truthful identification of the *switch* mechanism in active transporters. The methodological approach developed in this paper will be invaluable for a better interpretation of time-resolved data, uncovering key aspects behind the active transport by membrane proteins under functionally relevant conditions.

Acknowledgment. We thank Tzvetana Lazarova for invaluable discussions and suggestions, and Leonid Brown for critically reading the manuscript. This work was supported by grants from Japanese Ministry of Education, Culture, Sports, Science, and Technology to H.K. (19370067, 20657030, 20050015, 20108014).

Supporting Information Available: Part 1. Determination of the helix tilt angle changes in the M_2-to-N transition. Part 2. Determination of the Schiff Base (SB) axial orientation in

(75) Wolf, S.; Freier, E.; Gerwert, K. *ChemPhysChem* **2008**, *9*, 2772–2778.
(76) Zimányi, L.; Kulcsár, A.; Lanyi, J. K.; Sears, D. F., Jr.; Saltiel, J. *Proc. Natl. Acad. Sci. U.S.A.* **1999**, *96*, 4414–4419.
(77) Váró, G.; Lanyi, J. K. *Biochemistry* **1991**, *30*, 5016–5022.
(78) Cao, Y.; Brown, L. S.; Needleman, R.; Lanyi, J. K. *Biochemistry* **1993**, *32*, 10239–10248.
(79) Renthal, R.; Lanyi, J. K. *Biochemistry* **1976**, *15*, 2136–2143.
(80) Renard, M.; Delmelle, M. *Biophys. J.* **1980**, *32*, 993–1006.
(81) Miercke, L. J.; Betlach, M. C.; Mitra, A. K.; Shand, R. F.; Fong, S. K.; Stroud, R. M. *Biochemistry* **1991**, *30*, 3088–3098.
(82) Onufriev, A.; Smondyrev, A.; Bashford, D. *J. Mol. Biol.* **2003**, *332*, 1183–1193.
(83) Ferreira, A. M.; Bashford, D. *J. Am. Chem. Soc.* **2006**, *128*, 16778–16790.
(84) Luecke, H.; Schobert, B.; Richter, H. T.; Cartailler, J. P.; Lanyi, J. K. *J. Mol. Biol.* **1999**, *291*, 899–911.

the M_2 substate. Part 3. Interpretation of previous time-resolved X-ray scattering results. Part 4. Subtraction of the transient heat contribution and correction for the possible distortions introduced in the kinetics. Figure S1 - experimental kinetics used as a secondary constrain to obtain the intrinsic rate constants of the bR photocycle. Figure S2 - search for possible multiple kinetic solutions. Figure S3 - kinetic analysis of the bR photocycle forcing the L-to-M_1 and the M_1-to-M_2 transitions to be irreversible. Figure S4 - kinetic analysis of the bR photocycle forcing the M_2-to-N and N-to-O transitions to be irreversible. Figure S5 - intermediate difference IR spectra with confidence intervals, including the $M_2 - M_1$ difference spectrum. Figure S6 - deconvoluted $N - M_2$ difference spectrum. Figure S7. SB orientation change between M substates deduced from IR spectroscopy and several X-ray structures. Figure S8 - comparison of M accumulation in Oka et al.[64] experiments with our experimental conditions. Figure S9 - illustration of possible distortions introduced by the correction of the transient heat contribution on the kinetics. This material is available free of charge via the Internet al http://pubs.acs.org.

JA900334C